Catal Lett (2012) 142:809–815
DOI 10.1007/s10562-012-0826-0

Synthesis of SnO_2 Nanostructures and Their Application for Hydrogen Evolution Reaction

Hulin Zhang · Chenguo Hu · Siguo Chen · Kaiyou Zhang · Xue Wang

Received: 10 March 2012 / Accepted: 10 April 2012 / Published online: 26 April 2012

Abstract SnO_2 hierarchical architectures were synthesized with a surfactant-free hydrothermal synthesis route. We found that the acid or alkaline amount (HCl or NaOH) of the solution had a remarkable effect on the morphology of as-synthesized products. The SnO_2 nanostructures were selected as a support of Pt catalyst (Pt/SnO_2) for hydrogen evolution reaction (HER) in the acidic media. The influence of SnO_2 morphologies on the electrochemical performance has been investigated by cyclic voltammetry and linear sweeping voltammetry using the rotating disk electrodes. In addition, the effect on the catalytic activity in different electrolyte concentration was taken into account. Kinetic study shows that the HER on the Pt/SnO_2(flower) electrocatalyst gives a higher exchange current density and a lower overpotential in H_2SO_4 solution with high concentration.

Keywords SnO_2 nanostructures · Platinum · HER

1 Introduction

Nanostructured metallic oxides are considered to be important semiconductors which have attracted considerable interest due to their exceptional properties in optics, electronics, magnetics, and catalysis [1–4]. The properties and applications of such semiconductors are determined by the morphology, structure, and organization of nanostructured architectures to a great extent. Considerable efforts have been focused on the synthesis of a novel nanostructure with tailored morphology [5–7]. Tin oxide (SnO_2) is a stable and n-type wide band gap semiconductor with excellent optical and electrical properties. It is of great importance in a wide range of technological applications, such as gas sensors, optoelectronic devices, electrode materials and catalysts [8–11]. Besides, the hierarchical SnO_2 nanostuctures with larger specific surface area and porous structure have been paid more attentions because of their potential applications, especially in gas detection and catalysis [8, 12]. Morphological control of SnO_2 nanostructures is of great significance for systematic fundamental studies of crystal growth and for exploring new applications of nanostructures due to the interesting size- and shape-dependent properties [13]. Huang and coworkers and Pan' group reported poly(acrylic acid) and phenol formaldehyde resin assisted solvothermal method for synthesizing SnO_2 hierarchical structures [14, 15]. Our group also developed a hydrothermal process induced by salts to synthesize SnO_2 nanoflowers [16]. Nevertheless, to date, there is no literature available on that the amount of acid or alkaline (HCl or NaOH) in the solution had a remarkable effect on the morphology of as-synthesized SnO_2 hierarchical structures.

In addition, hydrogen is considered as an ideal fuel of the future because it is clean, has a high energy density and could be produced from renewable energy sources [17]. The electrolysis of water is a method of hydrogen production from renewable sources such as solar or wind energies. The efficiency of water electrolysis depends critically on catalyst materials. The most popular catalyst for H_2 evolution in acidic media is Pt noble metal [18]. To reduce the catalyst cost, recently, a lot of work has been carried out to develop new catalysts. One approach to cost reduction is to efficiently utilize Pt by distributing limited Pt nanoparticles on

H. Zhang · C. Hu (✉) · K. Zhang · X. Wang
Department of Applied Physics, Chongqing University, Chongqing 400044, People's Republic of China
e-mail: hucg@cqu.edu.cn

S. Chen
School of Chemical Engineering, Chongqing University, Chongqing 400044, People's Republic of China

a novel support [19, 20]. SnO_2 is widely used as catalyst support with good chemical and thermal stability. Accordingly, it is expected that hierarchical SnO_2 nanostructures with porous structures and larger specific surface area, which can provide more electrochemical active sites [21], can be applied in electrochemical hydrogen evolution.

In this paper, SnO_2 hierarchical architectures with different morphologies are prepared by one step hydrothermal reaction with surfactant-free approaches. The as-produced SnO_2 nanostructures are characterized by X-ray diffraction (XRD), field emission scanning electron microscopy (FESEM), transmission electron microscopy (TEM) and high resolution transmission electron microscopy (HRTEM). In addition, the as-prepared hierarchical nanostructures are also used as a support of Pt catalyst (Pt/SnO_2) for HER in the acidic media. The influences of SnO_2 morphologies and concentration of electrolyte on the electrochemical performance have been investigated by CV and LSV.

2 Experimental Section

2.1 Chemicals

Sodium stannate ($Na_2SnO_3{\cdot}3H_2O$), sodium hydroxide (NaOH), hydrochloric acid (HCl, 36 % by weight), sodium borohydride ($NaBH_4$), ethanol (C_2H_5OH), chloroplatinic acid ($H_2PtCl_6{\cdot}6H_2O$) and sulfuric acid (H_2SO_4) were purchased from Chongqing Chemical Reagent Company. Nafion and silver paste were purchased from Sigma-Aldrich and SPI Supplies. All chemicals were of analytical grade and deionized water was used throughout.

2.2 Synthesis of SnO_2 Nanocrystals

SnO_2 nanostructures were synthesized by the hydrothermal method. In a typical preparation: 0.266 g $Na_2SnO_3{\cdot}3H_2O$, 0–250 μL HCl (36 %) or 0–0.7 g NaOH, 10 mL deionized water and 10 mL absolute ethanol were put in a beaker, as shown in Table 1. After magnetic stirring for about 5 min, the reaction mixture was transferred into a Teflon-lined autoclave with 25 mL capacity. The vessel was sealed and heated at 200 °C for 24 h in an electric furnace. Then the autoclave was allowed to cool to room temperature naturally. Finally, the product was washed with deionized water several times and allowed to dry in ambient air for the further characterization.

Table 1 The samples synthesized by the hydrothermal method under different conditions

Samples	Additives	Morphologies
A	0.2 mL HCl	Nanorambutan
B	0.1 mL HCl	Nanorambutan
C	0	Nanorambutan
D	0.1 g NaOH	Nanoflower
E	0.2 g NaOH	Nanoflower
F	0.4 g NaOH	Nanoflower
G	0.6 g NaOH	Nanoflower

2.3 The Preparation and Characterization of Pt/SnO_2 Catalysts

The Pt/SnO_2 catalysts were prepared via the wet chemical routine reported previously [16]. X-ray powder diffraction (XRD) was taken to identify the crystalline phase of the as-prepared samples in a continuous mode over the range of 20–80°. Cu was used as the source of X-ray. The morphology of SnO_2 nanostructures and the Pt/SnO_2 nanostructures were characterized by FESEM (Nova 400 Nano SEM), TEM (TEM, JEOL4000EX) and HRTEM (HRTEM 400 kV, JEOL4000EX).

2.4 Electrochemical Measurements

Glassy carbon-rotating disk electrodes (0.071 cm^2) (MSRX SPEED CONTROL AFMSRX 466, which was purchased from Pine instrument company) were used as working electrodes by dropping the fixed quantity of the catalyst ink on the surface of the glassy carbon**.** The Pt loading on the electrode**s** was 0.13 mg cm^{-2}. CHI660D electrochemical analyzer, which was purchased from Shanghai Chenhua Instrument Co., LTD, was employed for electrochemical measurements, which were carried out with a conventional three-electrode electrochemical cell. Pt foil and Ag/AgCl (saturated KCl) were used respectively as the counter and reference electrodes. All the experiments were performed at room temperature (20 °C).

3 Results and Discussion

3.1 Characterization of the As-Prepared SnO_2 and Pt/SnO_2 Nanostructures

Typical XRD patterns of the samples obtained in different conditions are shown in Fig. 1. All the peaks can be indexed to the tetragonal phase of SnO_2 (JCPDS 41-1445) without any impurity peaks. It is seen that the peaks are weak and wide when prepared with the additive of HCl. However, the peaks become sharper and narrower with the additive of NaOH, indicating that the average size of the SnO_2 nanostructures becomes larger according to Scherrer's equation [22]. These results were confirmed by FESEM images.

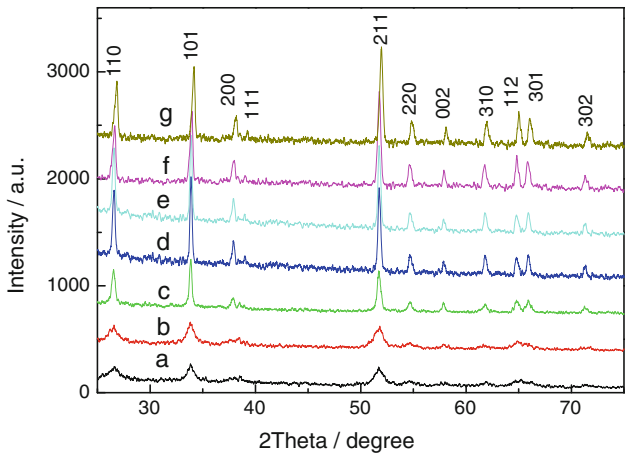

Fig. 1 XRD patterns of the SnO_2 samples prepared by adding different amount of HCl or NaOH, 0.2 mL (*a*), 0.1 mL (*b*) and 0.0 mL (*c*) HCl; 0.1 g (*d*), 0.2 g (*e*), 0.4 g (*f*) and 0.6 g (*g*) NaOH

Figure 2 shows typical FESEM images of SnO_2 nanostructures synthesized with the different additives. The FESEM image of sample a is shown in Fig. 2a, which exhibits rambutan-like morphology with the size of about 150 nm consisting of dense SnO_2 nanoparticles which assemble into the beautiful rambutan-like morphology. The rambutans adhere together into agglomeration, indicating the poor dispersity of the SnO_2 rambutans. The size of SnO_2 rambutans becomes larger with the decreasing amount of HCl, as shown in Fig. 2b, c. The SnO_2 nanorambutans can be obtained with the amount of HCl less than 200 μL. However, the morphology of the SnO_2 is flower-shaped and the nanorods self-assemble into nanoflowers when NaOH is added to the reaction mixture as shown in Fig. 2d–g. As the amount of NaOH increases from 0.2 to 0.6 g, SnO_2 nanostructures become more uniform and the diameter of SnO_2 nanoflowers consisting of the thinner nanorods become bigger, as shown in Fig. 2d–g. The SnO_2 nanoflowers are prepared with the additive of NaOH less than 0.6 g (when the amount of HCl is over 200 μL or the amount of the NaOH is over 0.6 g, no products can be obtained). The *insets* are the corresponding histograms of the size distribution. Figure 2h shows the energy dispersive X-ray spectrum (EDS) of the samples, which confirms the composition of tin and oxygen.

After being deposited by Pt, the SnO_2 nanostructures are covered by Pt nanoparticles. The FESEM images of the Pt/SnO_2(flower) catalyst and Pt/SnO_2(rambutan) catalyst are shown in Fig. 3a and b, respectively. Pt particles are deposited uniformly on SnO_2 flowers, while the Pt aggregates is found between SnO_2 rambutans due to the agglomeration of SnO_2 rambutans. The *inset* of Fig. 3a shows typical EDS results of the obtained Pt/SnO_2 nanostructures, further revealing that the samples contain Pt in addition to tin and oxygen. The details of the Pt/SnO_2(flower) catalysts are shown by TEM image in Fig. 3c and HRTEM image in Fig. 3d, respectively, which suggest a lot of Pt nanocrystals with sizes ranging from 5 to 8 nm distribute uniformly onto the surface of SnO_2 nanorods.

3.2 Electrochemical Measurement on the Pt/SnO_2 Electrodes

The stationary electrode cyclic voltammograms (CVs) taken in 0.5 M H_2SO_4 for the Pt/SnO_2(flower) and Pt/SnO_2(rambutan) electrocatalysts are shown in Fig. 4A. In the acid medium, there are two peaks at −0.126 and −0.024 V for the Pt/SnO_2(flower) electrocatalyst due to the hydrogen adsorption/desorption while there exist similar peaks at −0.141 and −0.035 V for the Pt/SnO_2(rambutan) electrocatalyst. The integral of adsorption and desorption peaks for the Pt/SnO_2(flower) catalyst are 0.81 and 0.86 V mA cm^{-2} and corresponding values of the Pt/SnO_2(rambutan) catalyst are 0.35 and 0.21 V mA cm^{-2}, respectively. Obviously, the peaks on the Pt/SnO_2(flower) electrode are much stronger than that on the Pt/SnO_2(rambutan) electrode, which suggests the Pt/SnO_2 (flower) catalyst has better catalytic activity. The electrochemical active surface (EAS) is calculated according to the area of hydrogen adsorption/desorption peaks [23]. The EAS is 57.2 m^2 g^{-1} for Pt/SnO_2(flower) and 21.1 m^2 g^{-1} for Pt/SnO_2(rambutan) in acidic media, indicating a more effective catalysis for the Pt/SnO_2(flower) catalyst due to the multidimensional hierarchical structure. The linear sweeping voltammograms (LSVs) for HER over the Pt/SnO_2(flower) electrocatalyst with the different rotation rates (1,600, 900, 400 and 0 rpm) are illustrated in Fig. 4B, indicating that with the increase of the rotation rate the corresponding current density increases. It is demonstrated that the obvious concentration polarization on Pt/SnO_2 (flower) electrocatalyst and the concentration polarization decreases as the rotation rate increases. The similar curves obtained on the Pt/SnO_2(rambutan) catalyst are shown in Fig. 4C. The curve measured on the Pt/SnO_2(flower) electrocatalyst shows a slightly lower overpotential compared to that on the Pt/SnO_2(rambutan) electrocatalyst. Also, the current density on the Pt/SnO_2(flower) electrocatalyst is higher than that on Pt/SnO_2(rambutan) catalyst at the fixed potential, which is consistent with the results from CVs.

The higher catalytic activity for HER for the Pt/SnO_2 (flower) electrocatalyst is due to more electrochemical active sites and larger specific surface area provided by the multidimensional catalyst in which the hierarchical SnO_2 flowers were coated uniformly with Pt nanoparticles. The Pt/SnO_2(rambutan) electrocatalyst, in contrast, has less spatial structure owning to the agglomeration of the SnO_2 rambutans as shown in Fig. 3b. In addition, the radial

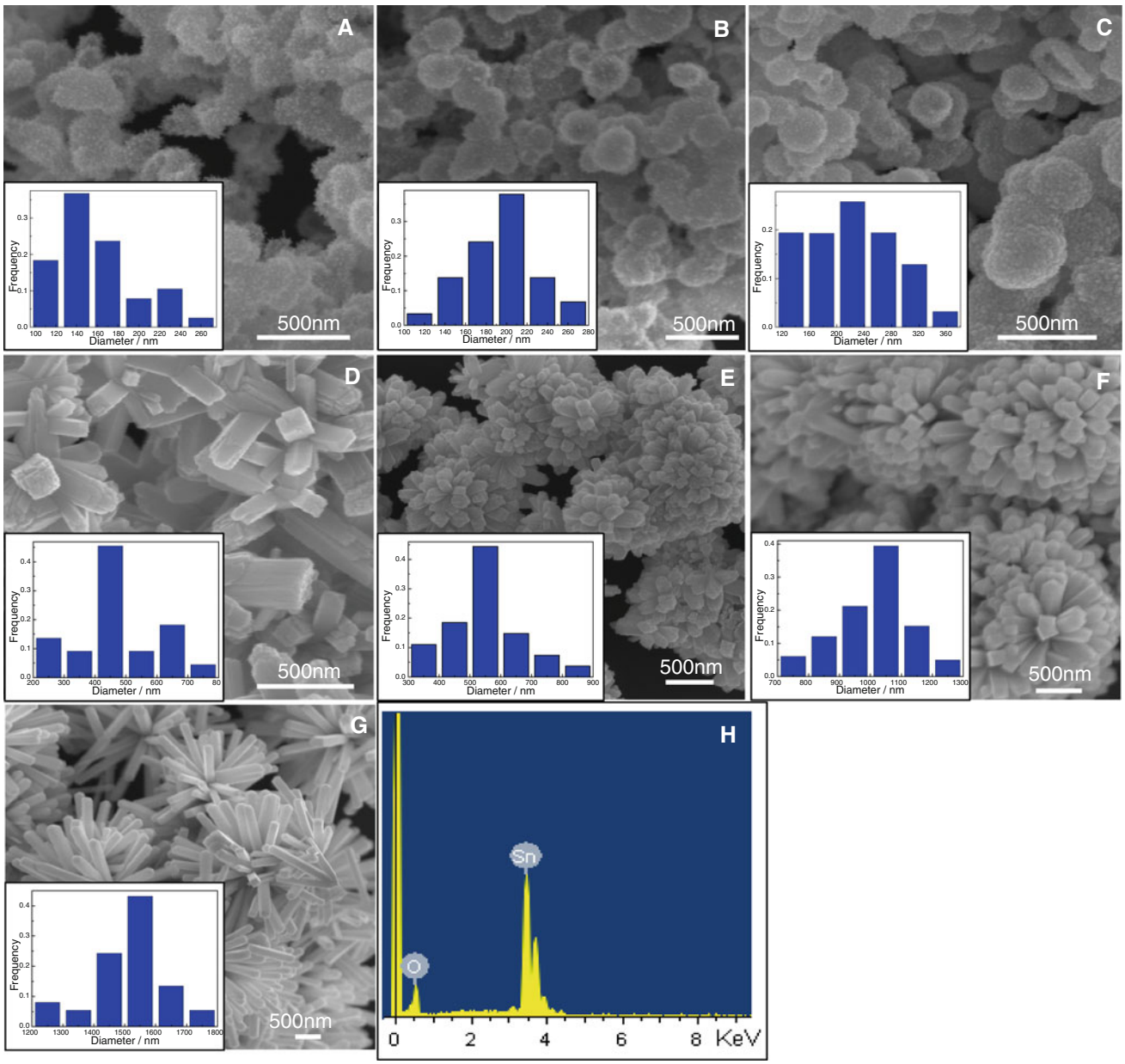

Fig. 2 FESEM images of the SnO_2 samples prepared with different amount of HCl or NaOH. 0.2 mL of HCl (**a**, sample a), 0.1 mL of HCl (**b**, sample b), without HCl or NaOH (**c**, sample c), 0.1 g of NaOH (**d**, sample d), 0.2 g of NaOH (**e**, sample e), 0.4 g of NaOH (**f**, sample f) and 0.6 g of NaOH (**g**, sample g). The EDS spectrum (**h**). The *insets* are the corresponding histograms of the size distribution

channels and the porous structure in the Pt/SnO_2(flower) catalyst also shorten the electronic diffusion distance and facilitate the diffusion of liquid reactants into the catalyst interface, resulting in reduction of liquid sealing effect greatly. The reduction of liquid sealing effect in turn increases the renewable active surface area for HER [24].

Stationary electrode LSVs and Tafel plots of the Pt/SnO_2(flower) electrocatalyst were obtained in H_2SO_4 solution with different concentrations to explore quantitatively the electrochemical activity for HER in the acid electrolytes. Figure 5A shows the influence of electrolyte concentration on the catalysis of Pt/SnO_2(flower) electrocatalyst for HER, indicating that the polarization overpotential is highly relevant to the electrolyte concentration. The overpotential drops gradually with the increase of the H_2SO_4 concentrations from 0.1 to 2.0 M. The onset potential of HER is −106.39 mV in 2.0 M, −127.74 mV in 1.0 M, −142.27 mV in 0.5 M and −167.63 mV in 0.1 M solution, respectively. The onset potential in 2.0 M H_2SO_4 is 50 mV more positive than that in 0.1 M H_2SO_4 solution. The higher current density for HER also can be observed at higher H_2SO_4 concentrations. The Tafel plots

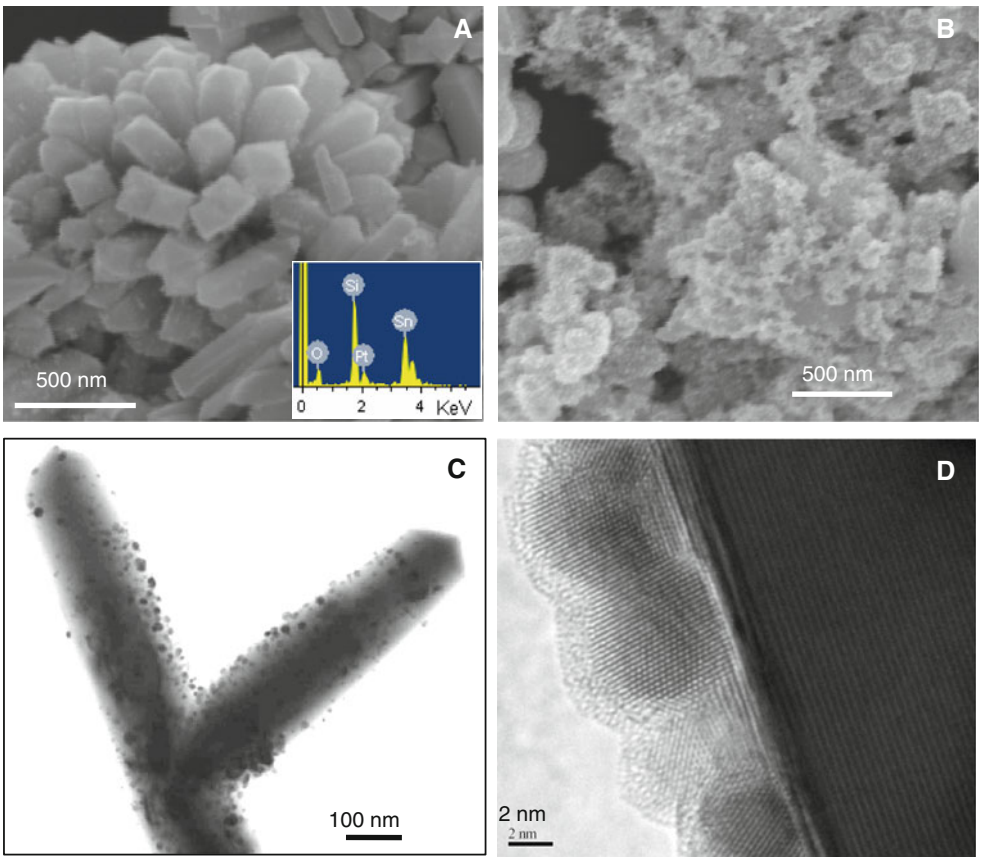

Fig. 3 FESEM images of Pt catalysts supported by the SnO_2 flowers (**a**), SnO_2 rambutans (**b**), TEM image of the Pt/SnO_2(flower) catalyst (**c**) and HRTEM image of Pt/SnO_2(flower) catalyst (**d**). The *inset* of a is the EDS spectrum of the Pt/SnO_2 catalyst

of Pt/SnO_2(flower) electrocatalyst in different concentrations of H_2SO_4 solution are shown in Fig. 5B. The Tafel slope was calculated from the linear portion of the plot in the voltage range from−0.08 to −0.18 V. The exchange current density of HER, $i°$, which is a measure of the intrinsic electron transfer activity in both cathodic and anodic directions at equilibrium in dynamic electrochemistry, can be calculated by the intercept and slope of the Tafel plots through the Tafel extrapolation technique [25]. The corresponding kinetic parameters, which are calculated from the curves in Fig. 5B, are listed in Table 2.

Obviously, the concentration of H_2SO_4 solution has a significant effect on HER activity on Pt/SnO_2(flower) electrode. The onset potential decreases monotonically from −106.39 to −167.63 mV as the acid concentration decreases from 2.0 to 0.1 M, demonstrating the enhancement of the electrocatalytic activity of Pt/SnO_2(flower) electrocatalyst. The increase of the exchange current density (i_0) shown in column **4** is notable at higher electrolyte concentrations, which exhibits the range from 0.07 mA cm^{-2} in 0.1 M H_2SO_4 solution to 1.13 mA cm^{-2} in 2.0 M H_2SO_4 solution. The values of the exchange current density with the concentration correction are similar to each other as shown in column **5** (i_0^*) in Table 2. As the concentration increased from 0.1 to 2 M, the exchange current density with the concentration correction increased from 0.46 to 0.64 mA cm^{-2}. It is proved that the concentration polarization on Pt/SnO_2(flower) electrocatalyst is critical and a higher concentration of H_2SO_4 solution is preferable for the HER. The improvement in the kinetics of the HER in H_2SO_4 solution at higher concentrations is the evidence that the concentration polarization decreases with the increase of the H_2SO_4 concentration [19].

4 Conclusions

Tunable synthesis of SnO_2 nanostructures has been achieved via hydrothermal method without using any surfactants. The morphologies of rambutan and flower can be obtained by the adjustment of acidity of reaction solution. The Pt nanoparticles with a size of 5–8 nm have been uniformly loaded on the SnO_2(flower) supports, which is adopted as the electrocatalyst for hydrogen

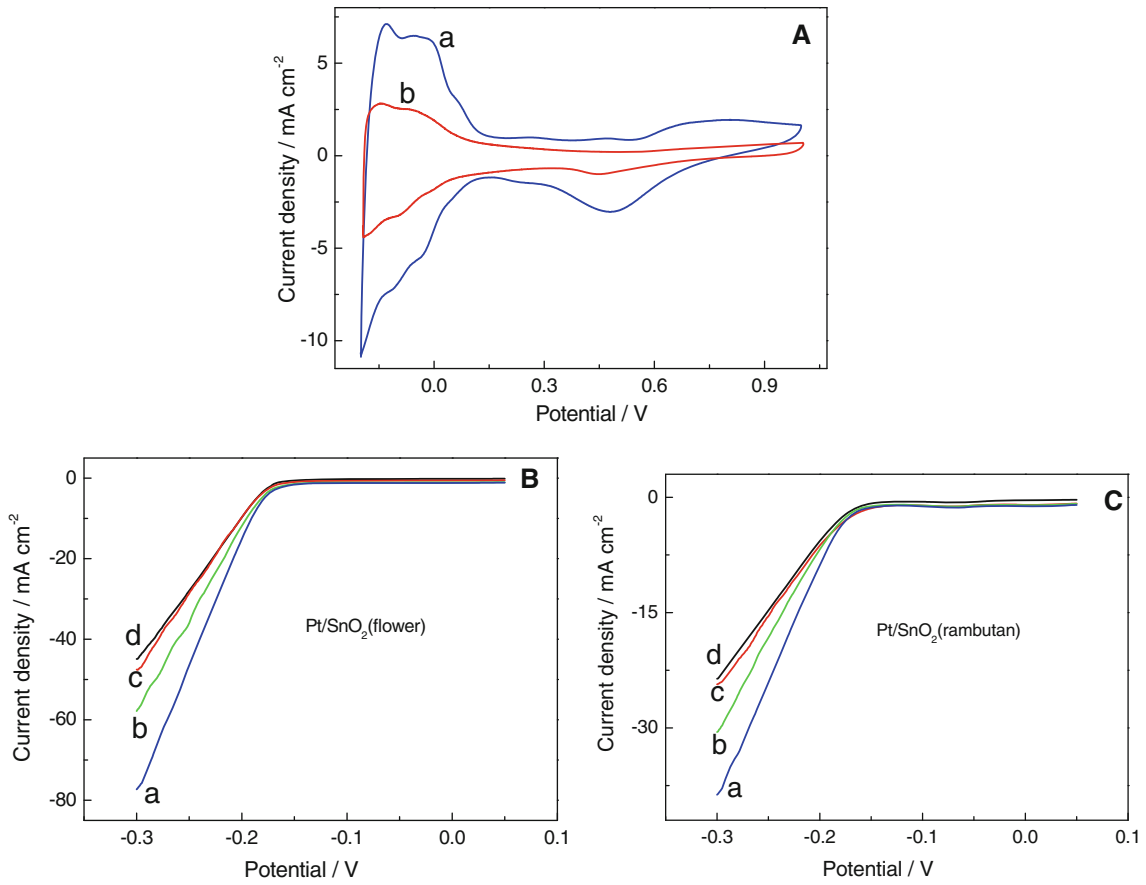

Fig. 4 CVs (**A**) of the flower SnO_2 support (*a*) and rambutan SnO_2 support (*b*) Pt catalyst in 0.5 M H_2SO_4 solution with the scan rate of 50 mVs^{-1}. LSVs (**B**, **C**) of the Pt/SnO_2(flower) catalyst and Pt/SnO_2(rambutan) catalyst in 0.5 M H_2SO_4 solution with the scan rate of 10 mVs^{-1} at the rotation rates of 1600 rpm (*a*), 900 rpm (*b*), 400rpm (*c*) and 0 (*d*), respectively

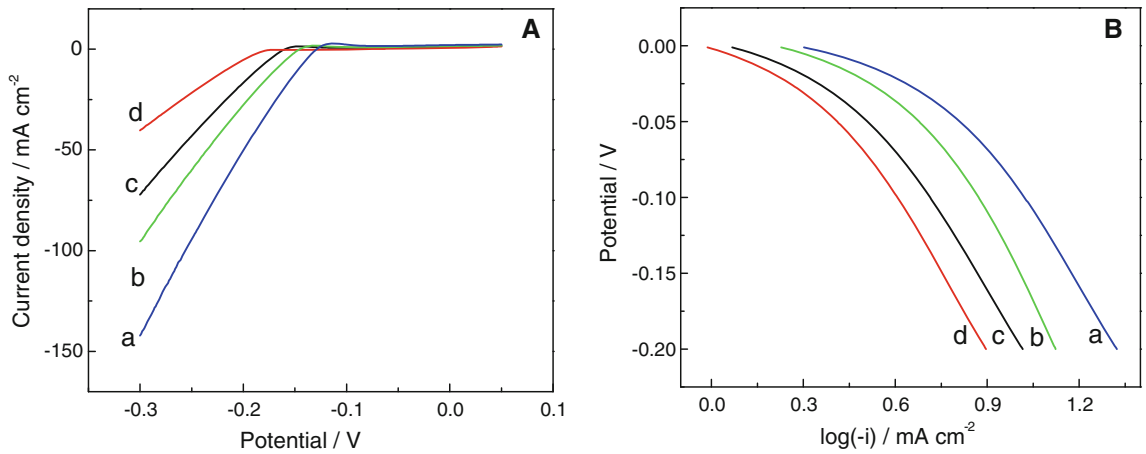

Fig. 5 LSVs (**A**) and Tafel plots (**B**) of the Pt/SnO_2(flower) electrode in H_2SO_4 solutions at the concentrations of H_2SO_4 of 2.0 (*a*), 1.0 (*b*), 0.5 (*c*) and 0.1 M (*d*) with the scan rate of 10 mV s^{-1}, respectively

evolution reaction in acidic media. The voltammetric results indicated that Pt/SnO_2(flower) electrocatalyst exhibits higher activity for HER due to its larger specific surface area and porous structure. It suggests that Pt/SnO_2(flower) electrocatalyst has a potential application in hydrogen generation.

Table 2 Comparison of kinetic parameters for HER on the Pt/SnO_2(flower) electrode in different concentrations of H_2SO_4 solutions

Concentrations of H_2SO_4 solutions (M)	Onset potential (mV)	Tafel slope (mV/dec)	$-i_0$ (mA cm^{-2})	$-i_0^*$ (mA cm^{-2})
0.1	−167.63	−111.31	0.07	0.46
0.5	−142.27	−99.74	0.25	0.55
1.0	−127.74	−82.67	0.48	0.58
2.0	−106.39	−71.66	1.13	0.64

Acknowledgments This work is supported by the NSFC (6097 6055), SRFDP (20110191110034), Project (WLYJSBJRCTD201101) of the Innovative Talent Funds for 985 Project, and the Large-Scale Equipment Sharing Fund of Chongqing University.

References

1. Morles AM, Lieber CM (1998) Science 279:208
2. He JH, Hsin CL, Liu J, Chen LJ, Wang ZL (2007) Adv Mater 19:781
3. Hays J, Punnoose A, Baldner R, Engelhard MH, Peloquin J, Reddy KM (2005) Phys Rev B 72:075203
4. Zhao J, Yue YH, Zhai DW, Miao CX, Shen JY, He HY, Hua WM, Gao Z (2009) Catal Lett 133:119
5. Wang X, Zhuang J, Peng JQ, Li YD (2005) Nature 437:121
6. Liu XG (2009) Angew Chem Int Ed 48:3018
7. Li L, Yang YW, Li GH, Zhang LD (2006) Small 2:548
8. Lee JS, Sim SK, Min B, Cho K, Kim SW, Kim S (2004) J Cryst Growth 267:145
9. Xu G, Zhang YW, Sun X, Xu CL, Yan CH (2005) J Phys Chem B 109:3269
10. Sugimoto H, Tsukube H, Tanaka K (2004) Eur J Inorg Chem 23:4550
11. Enesca A, Andronic L, Duta A (2012) Catal Lett 142:224
12. Jia TK, Wang WM, Long F, Fu ZY, Wang H, Zhang QJ (2009) J Phys Chem C 113:9071
13. Burda C, Chen X, Narayanan R, El-Sayed MA (2005) Chem Rev 105:1025
14. Cheng GE, Wang JM, Liu XW, Huang KX (2006) J Phys Chem B 110:16208
15. Wang H, Xu JQ, Pan QY (2010) Cryst Eng Comm 12:1280
16. Zhang HL, Hu CG, He XS, Liu H, Du GJ, Zhang Y (2011) J Power Sources 196:4499
17. Penner SS (2006) Energy 31:33
18. Seto K, Iannelli A, Love B, Lipkowski J (1987) J Electroanal Chem 226:351
19. Wu M, Shen PK, Wei ZD, Song SQ, Nie M (2007) J Power Sources 166:310
20. Ham DJ, Ganesan R, Lee JS (2008) Int J Hydrogen Energy 33:6865
21. Wang H, Liang QQ, Wang WJ, An YR, Li JH, Guo L (2011) Cryst Growth Des 11:2942
22. Scherrer P, Gottingen NGW (1918) Math-Phy KI 2:96
23. Pozio A, De Francesco M, Cemmi A, Cardellini F, Giorgi L (2002) J Power Sources 105:13
24. Xie FY, Tian ZQ, Meng H, Shen PK (2005) J Power Sources 141:211
25. Lee JS, Volpe L, Ribeiro FH, Boudart M (1988) J Catal 112:44